Surface Effect Ship with Four Air Cushions
Part II: Roll and Pitch Damping ⋆

Ola M. Haukeland * Vahid Hassani **,***,1
Øyvind Auestad ****

*Department of Marine Technology,
Norwegian Univ. of Science and Technology,
Trondheim, Norway.

** Department of Mechanical, Electronics and Chemical Engineering,
Oslo Metropolitan University,
Oslo, Norway (e-mail: vahid.hassani@oslomet.no).

*** Department of Ships and Ocean Structures, SINTEF Ocean,
Trondheim, Norway.

**** Umoe Mandal AS,
Mandal, Vest-Agder, Norway.

Abstract: This paper introduce damping of roll and pitch motion on a Surface Effect Ship (SES) in low vessel speeds. The SES consist of two side-hulls, a reinforced rubber bow and stern seal skirt system and four air cushion. The air cushions can lift up to 90 % of the total vessel mass depending on the output of the controller. The pressure in the air cushions are controlled using feedback from gyros which results in heavily reduced motions in roll and pitch. The effectiveness of the proposed system is examined through numerical simulation in a high fidelity simulator developed in a companion article (Ola M. Haukeland, Hassani, and Auestad 2019).

Keywords: Surface Effect Ship, Split Cushion, Roll and Pitch Damping

1. INTRODUCTION

The Surface Effect Ship (SES) is a seagoing vehicle that traditionally operates at high-speed at the interface area between air and water. This is possible due lift fan(s) that blows air into an air cushion and thereby pressurizing it. The air cushion is a trapped volume underneath the vessel enclosed by the water surface, side-hulls, bow and stern seals. The seals inhabit the same structural properties found on the seals of a hovercraft but with a different geometry. Figure 1 gives an illustration of a SES cross-section, as seen from the side.

The SES discussed in this paper is slightly modified compared to the traditional SES since the volume underneath the vessel is divided into four air cushions and not one. In addition to inheriting the high-speed, the SES discussed in this paper also present roll and pitch motion control at low speeds which is the topic of this work. Roll and pitch damping is possible by altering the pressures individual in the four chambers. For instance, if the two starboard cushions have higher pressure then on the port side, then the motion induced by a sea wave crest encountering the port deck-side can be damped.

Though this project is done in collaboration with Umoe Mandal, the properties of the simulated model are generic.
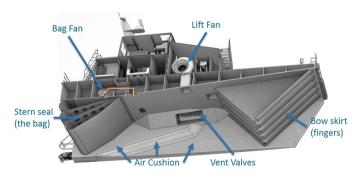

Fig. 1. Cross section of a SES. Illustration by Umoe Mandal.

The results given in chapter 4 do not represent any one of Umoe Mandal's vessels in particular.

1.1 Motivation

The rough seas surrounding offshore structures such as oil platforms, oil-rigs and wind turbines provide a challenge for both crew transport and offshore structure inspections. The use of surface effect ships has emerged as a competitive alternative to helicopter transport, proving high levels of safety, comfort, fuel efficiency and overall reduced cost of offshore logistics, Mandal 2018. The main challenge for sea transport is safety at crew transfer and ride comfort at high transit speeds. Increased motion control and motion damping provides the solution to these challenges, and

[1] Corresponding Author.

contributes to an expand of the operational window for marine vessels at harsh weather conditions.
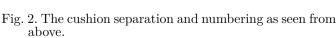
1.2 Simulation environment

The numerical simulations will be carried out in a process plant model referred to as SESSim, Ola M. Haukeland, Hassani, and Auestad 2019. This is a mathematical model implemented in MATLAB®/Simulink®, created to accurately depict the dynamics of the surface effect ship. The model is expanded to include the four cushion solution, and also provides the basis for the derivation of the control plant model in section 2.

1.3 SES Cushion-control

Other systems for controlling a SES-vessel by manipulating the cushion pressure are already developed and in use, among them is the ride control system and the boarding control system. The ride control system was first featured in Kaplan and Davis 1978, and has since been further developed by Sørensen and Egeland 1995. The purpose of the system is to create a more smooth ride at high transit velocities. The system provides active damping of vertical motions by manipulating and reducing the cushion pressure fluctuations caused by rough sea. The boarding control system has been developed by Ø. F. Auestad 2015; Hassani, Fjellvang, and Auestad 2019. The main use of the boarding control system is to reduce the movements of the vessel's bow, so that it is possible to secure safer transfer from the ship to offshore structures, specifically, offshore wind-turbines. The boarding control system relies on manipulating the pressure of the single cushions to counteract the wave-induced motions.

1.4 Cushion division

In this paper, we consider a SES design in which the single cushion is divided into four sections by the use of solid walls or inflatable separators. The division and subsequent cushion numbering can be seen in figure 2. The implementation of the four chambers solution using inflatable bags allows for usage of a the traditional one-cushion solution when the four cushion division is not needed.

Fig. 2. The cushion separation and numbering as seen from above.

2. MATHEMATICAL MODEL

A non-linear high fidelity process plant model of SES with split cushion is derived in Ola M. Haukeland, Hassani, and Auestad 2019. In this section, a linear time-invariant (LTI) model is presented for the system to act as a control plant model. The presented LTI model is result of linearization of the model developed in Ola M. Haukeland, Hassani, and Auestad 2019

2.1 Cushion pressure dynamics

The cushion pressure is considered to be uniform within each cushion chamber. The pressure in each chamber is denoted p_{c_i} and can be expressed as shown in equation 1.

$$p_{c_i}(t) = p_a + p_{u_i}(t) \tag{1}$$

Here p_a is the atmospheric pressure, while $p_{u_i}(t)$ is the uniform excess pressure. When the vessel is in equilibrium, meaning it has no movement, the excess pressure p_{u_i} is defined as the equilibrium pressure, p_{0_i}. The excess pressure can be written in a non-dimensional form as μ_u, where

$$\mu_{u_i}(t) = \frac{p_{u_i}(t) - p_0}{p_0} \tag{2}$$

As the vessel is designed for a single cushion solution with the option of four cushions, and the walls of the cushions are considered thin, assuming that the equilibrium pressure p_0 is the same for all of the cushions is reasonable. The volume of air inside each cushion will vary with the elevation of the water surface as well as the heave, pitch and roll of the vessel. The interaction between the volume, air leakage, wave volume pumping of the cushions and the equations of motion for the vessel can be expressed as shown in equation 3. This equation is based on the uniform pressure equation derived in Sørensen and Egeland 1995. The equation has since been altered and expanded to fit the current system and four cushion solution. Note that the equation is a linearization, and is only valid for small changes in pressure around the linearization point at p_0.

$$
\begin{aligned}
K_{1_i}\dot{\mu}_{u_i}(t) &+ K_3\mu_{u_i}(t) + \rho_{c0}A_{c_i}\dot{\eta}_3(t) \\
&+ \rho_{c0}A_{c_i}y_{cp_i}\dot{\eta}_4(t) - \rho_{c0}A_{c_i}x_{cp_i}\dot{\eta}_5(t) \\
&= K_{2_i}\Delta A_{2_i}^{ctrl}(t) + \rho_{c0}\dot{V}_{0_i}(t)
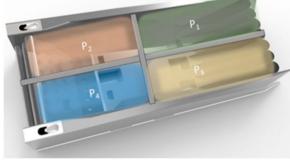\end{aligned}
\tag{3}
$$

Here A_{c_i} is the area of cushion i, projected onto the water plane. The constants x_{cp_i} and y_{cp_i} are the centers of pressure, or center of area for each of the cushions. The constants K_{1_i}, K_{2_i} and K_3 are calculated as shown in the equations below.

$$K_{1_i} = \frac{\rho_{c0}V_{c0_i}}{\gamma(1 + \frac{p_a}{p_0})} \tag{4}$$

$$K_{2_i} = \rho_{c0}c_{n_i}\sqrt{\frac{2p_0}{\rho_a}} \tag{5}$$

$$K_3 = \rho_{c0}\sum_{j=1}^{q}\left(\frac{Q_{0j}}{2} - p_0\frac{\partial Q}{\partial p}\Big|_{0j}\right) \tag{6}$$

Here ρ_a is the atmospheric air density, and p_a is the atmospheric pressure. Similarly, p_0 and ρ_0 is the cushion equilibrium pressure and air density, while γ is the ratio of specific heat for air. Q_{0j} is the air flow rate at the fore-mentioned equilibrium pressure, while $\frac{\partial Q}{\partial p}|_{0j}$ is the corresponding linearized fan slope around the equilibrium point $0j$. Here subscript j denotes the numbering of

the fans, providing air-flow Q. Lastly, c_n is the leakage coefficient, which is dependent on the shape of the leakage area. $\dot{V}_{0_i}(t)$ is the wave volume pumping, which is further explained and derived in **Paper1** but can be expressed as shown in equation 7. Note that V_{c0_i} denotes the cushion volume for cushion i at the equilibrium pressure, and is not related to the wave volume pumping.

$$\dot{V}_{0_i}(t) = \int_{y_{1_i}}^{y_{2_i}} \int_{L_{1_i}}^{L_{2_i}} \dot{\zeta}(x,y,t)dA \quad (7)$$

$$V_{0_i}(t) = \int_{y_{1_i}}^{y_{2_i}} \int_{L_{1_i}}^{L_{2_i}} \zeta(x,y,t)dA \quad (8)$$

Here y_{1_i} and y_{2_i} constitute the width of cushion i, while L_{1_i} to L_{2_i} constitutes the length of cushion i, measured at the current water-level. $\dot{\zeta}(x,y,t)$ is the function expressing the rate of change in the wave elevation at position x and y, at time t. This rate of change can be expressed as shown in equation 9, and is further detailed in **Paper1**

$$\dot{\zeta}(x,t) = \bar{\zeta}\omega \cos\left(\omega t + \epsilon - k(x\cos(\chi) + y\sin(\chi))\right) \quad (9)$$

2.2 Equations of motion

Only the forces in heave, roll and pitch will be of relevance to the control and simulations of the vessel dynamics in this paper. The vessel is considered stationary, such that the forces and moments in surge, sway and yaw will be negligible. The sum of forces acting on the vessel can be split into two components. Forces generated by the excess pressure in the cushions, and forces generated as a result of the buoyancy and hydrodynamic properties of the hull. Equations 10 through 12 express the forces and moments generated by the cushions in heave, roll and pitch.

$$F_{3_c}(t) = \sum_{i=1}^{4} -p_0 \mu_{u_i}(t) A_{z_i} \quad (10)$$

$$M_{4_c}(t) = \sum_{i=1}^{4} -y_{cp_i} p_0 \mu_{u_i}(t) A_{z_i} \quad (11)$$

$$M_{5_c}(t) = \sum_{i=1}^{4} x_{cp_i} p_0 \mu_{u_i}(t) A_{z_i} \quad (12)$$

Equations 13 through 15 express the equations of motion for the vessel. The hydrodynamic forces acting on the vessel are expressed through the first three terms on the left hand side of the equations. These forces and moments and the corresponding movements of the vessel can be stated as a mass-spring-damper system for each of the degrees of freedom.

$$(m + A_{33})\ddot{\eta}_3(t) + B_{33}\dot{\eta}_3 + C_{33}\eta_3 + F_{c_3}(t) = F_3^e(t) \quad (13)$$

$$(I_{44} + A_{44})\ddot{\eta}_4(t) + B_{44}\dot{\eta}_4 + C_{44}\eta_4 + M_{c_4}(t) = M_4^e(t) \quad (14)$$

$$(I_{55} + A_{55})\ddot{\eta}_5(t) + B_{55}\dot{\eta}_3 + C_{55}\eta_5 + M_{c_5}(t) = M_5^e(t) \quad (15)$$

The forces and moments $F_3^e(t)$, $M_4^e(t)$ and $M_5^e(t)$ are excitation forces and moments caused by waves and other external forces. The constant m represents the vessel mass, and the constants A, B and C represents the hydrodynamic added mass, the potential damping and restoring coefficient for the mass-spring-damper motion

of the vessel. Their subscripts 3, 4 and 5 denote the movements in heave, roll and pitch, respectively. Lastly the vessel inertia governing the roll and pitch motion of the vessel is given as I. The values for these constants are been computed in ShipX and Veres, and have been provided and Umoe Mandal.

2.3 State space representation

The equations of motion can be represented in the linear time-invariant state-space form shown in 16 and 17.

$$\dot{\boldsymbol{x}}(t) = \boldsymbol{A}\boldsymbol{x}(t) + \boldsymbol{B}\boldsymbol{u}(t) + \boldsymbol{E}\boldsymbol{\omega}(t) \quad (16)$$

$$\boldsymbol{y}(t) = \boldsymbol{C}\boldsymbol{x}(t) \quad (17)$$

Here, $\boldsymbol{x}(t)$ is the state vector, which represents the relevant degrees of freedom of the vessel. The representation of the vector $\boldsymbol{x}(t)$ is listed in the table below. $\boldsymbol{u}(t)$ is the control input, which will be further discussed in section 3. $\boldsymbol{\omega}(t)$ is the disturbance vector, which comprises of external forces and disturbances. $\boldsymbol{y}(t)$ is the output vector, and holds the values for any measured states such as data from accelerometers or gyros. The expressions for the matrices $\boldsymbol{A}$, $\boldsymbol{B}$, $\boldsymbol{E}$ and $\boldsymbol{C}$ can be found in Ola Mosebø Haukeland 2019.

States $\boldsymbol{x}(t)$		
State	Description	Symbol
$x_1(t)$	Heave position	η_3
$x_2(t)$	Roll angle	η_4
$x_3(t)$	Pitch angle	η_5
$x_4(t)$	Heave velocity	$\dot{\eta}_3$
$x_5(t)$	Roll velocity	$\dot{\eta}_4$
$x_6(t)$	Pitch velocity	$\dot{\eta}_5$
$x_7(t)$	Non-dim. pressure, chamber 1	μ_{u_1}
$x_8(t)$	Non-dim. pressure, chamber 2	μ_{u_2}
$x_9(t)$	Non-dim. pressure, chamber 3	μ_{u_3}
$x_{10}(t)$	Non-dim. pressure, chamber 4	μ_{u_4}

States $\boldsymbol{y}(t)$		
State	Description	Symbol
$y_1(t)$	Roll angle	η_4
$y_2(t)$	Pitch angle	η_5
$y_3(t)$	Heave velocity	$\dot{\eta}_3$
$y_4(t)$	Roll velocity	$\dot{\eta}_4$
$y_5(t)$	Pitch velocity	$\dot{\eta}_5$
$y_6(t)$	Pressure, chamber 1	p_{c_4}
$y_7(t)$	Pressure, chamber 2	p_{c_4}
$y_8(t)$	Pressure, chamber 3	p_{c_4}
$y_9(t)$	Pressure, chamber 4	p_{c_4}

3. CONTROLLER DESIGN

We wish to device a simple but reliable controller which ultimately can be applied to a real vessel similar to the one described by our model. We desire to control the roll and pitch of the vessel, and so a simple (partial-)state feedback controller is applied. The control law is formulated as shown in equation (18) below.

$$\boldsymbol{u}(t) = -\boldsymbol{K}\boldsymbol{x}(t) + \boldsymbol{\beta} \quad (18)$$

The controller output, $\boldsymbol{u}(t)$, returns the opening percentages of the cushion ventilation valves. A controller output of 100 reads 100% opening on the vent valve, and thus the corresponding cushion pressure is minimized. $\boldsymbol{\beta}$ is a constant matrix signifying the bias of the ventilation valve louvers. The bias essentially states how much lift the vessel should have when no feedback is present. The structure of the control output matrix is shown below. The subscripts

denote the ventilation valve louvers corresponding to the equally numbered cushion chamber.

$$\boldsymbol{u}(t) = [u_1(t) \ u_2(t) \ u_3(t) \ u_4(t)] \quad (19)$$

3.1 Stability of the closed loop system

An unstable system can easily lead to unexpected and undesired responses. For physical systems, such responses can easily produce dangerous and harmful situations. Thus, providing a stability proof for the controlled system gives an assurance that the controlled system will only act in a certain way, namely converging towards the equilibrium states of $\boldsymbol{x_0} = 0$.

Stability of unperturbed system   The unperturbed closed loop system, that is $\boldsymbol{E}\boldsymbol{\omega}(t) = 0$, can be said to be exponentially stable around $\boldsymbol{x_0}$ if the closed loop system matrix, $\boldsymbol{A}_{cl}$ is Hurwitz. This means that all the eigenvalues of $\boldsymbol{A}_{cl}$ have strictly negative real parts, i.e $\mathbb{R}(\lambda_i) < 0$. By inserting the expression of our chosen controller in (18) into the unperturbed state space representation of our system in (16), the closed loop system can be expressed as

$$\dot{\boldsymbol{x}}(t) = \boldsymbol{A}\boldsymbol{x}(t) - \boldsymbol{B}\boldsymbol{K}\boldsymbol{x}(t) + \boldsymbol{B}\boldsymbol{\beta} = \boldsymbol{A}_{cl}\boldsymbol{x}(t) + \boldsymbol{B}\boldsymbol{\beta} \quad (20)$$

where $\boldsymbol{A}_{cl} = \boldsymbol{A} - \boldsymbol{B}\boldsymbol{K}$. A general expression for the values of $\boldsymbol{K}$ which create a stable closed loop system can be devised by choosing an appropriate Lyapunov function, $\boldsymbol{V}(x)$ through use of the Lyapunov equation. Due to the size of the matrix $\boldsymbol{A}_{cl}$ and the number of unique gains in the $\boldsymbol{K}$-matrix, such a generalization will become long and tedious. Thus we settle for showing that the selected gains in section 3 will provide a stable closed loop system. The eigenvalues for the closed loop system are calculated numerically in MATLAB®. The resulting eigenvalues all have negative real parts. Thus the closed loop unperturbed system will converge exponentially fast towards the equilibrium states of $\boldsymbol{x_0}$.

Robustness of perturbed system   As the purpose of the system will be to counteract disturbances, the perturbed system, where $||\boldsymbol{E}\boldsymbol{\omega}(t)|| \neq 0$, must be shown to be robust. That is, small disturbances will not result in large steady-state deviations from the equilibrium. The perturbations affecting the vessel are time dependent, and do not stop as the system reaches it's equilibrium point, thus the perturbations can be seen as non-vanishing. This means that we can no longer expected the system to converge at the origin as $t \to \infty$. The best we can hope for is that the system response will be bounded by some small bound, if the disturbance is small, Khalil 2014. The closed loop perturbed system can be written as

$$\dot{\boldsymbol{x}}(t) = \boldsymbol{A}_{cl}\boldsymbol{x}(t) + \boldsymbol{E}\boldsymbol{\omega}(t) + \boldsymbol{B}\boldsymbol{\beta} \quad (21)$$

The Lyapunov function candidate for the system, $\boldsymbol{V}(x)$, is set as

$$\boldsymbol{V}(x) = \boldsymbol{x}^T \boldsymbol{P} \boldsymbol{x} \quad (22)$$

Differentiating $\boldsymbol{V}(x)$ with respect to time will provide an expression for the direction of the trajectory of the system. Thus if $\dot{\boldsymbol{V}}(x)$ is negative for all x, the system will be stable. $\dot{\boldsymbol{V}}(x)$ can be derived as

$$\begin{aligned} \dot{\boldsymbol{V}}(x) &= \boldsymbol{x}^T \boldsymbol{P} \dot{\boldsymbol{x}} + \dot{\boldsymbol{x}}^T \boldsymbol{P} \boldsymbol{x} \\ &= -\boldsymbol{x}^T \boldsymbol{Q} \boldsymbol{x} + \boldsymbol{x}^T \boldsymbol{P} \boldsymbol{E} \boldsymbol{\omega} + \boldsymbol{\omega}^T \boldsymbol{E}^T \boldsymbol{P} \boldsymbol{x} \end{aligned} \quad (23)$$

where

$$-\boldsymbol{Q} = \boldsymbol{P} \boldsymbol{A}_{cl} + \boldsymbol{A}_{cl}^T \boldsymbol{P} \quad (24)$$

Equation (24) is called the Lyapunov equation. If there exists a solution for the Lyapunov equation where both

$\boldsymbol{P}$ and $\boldsymbol{Q}$ are square positive definite matrices, that is $\boldsymbol{P} = \boldsymbol{P}^T > 0$ and $\boldsymbol{Q} = \boldsymbol{Q}^T > 0$, then $\dot{\boldsymbol{V}}(x)$ for the unperturbed will be negative, and the system will be stable. Since the system is perturbed, $\boldsymbol{Q}$ must satisfy the inequality shown below.

$$-\boldsymbol{Q} \leq \boldsymbol{P} \boldsymbol{E} \boldsymbol{\omega} + \boldsymbol{\omega}^T \boldsymbol{E}^T \boldsymbol{P} \quad (25)$$

Values for $\boldsymbol{P}$ and $\boldsymbol{Q}$ can be calculated from the unperturbed system. Given that the values for the disturbance, $\boldsymbol{\omega}$, are small enough to satisfy the inequality in (25), the perturbed closed loop system will produce a bounded response. Lemma 9.2 in Khalil 2014 can be applied as the nominal system has exponential stability about x_0, and because the Lyapunov function candidate for the nominal system, chosen in (22), satisfy the inequalities (26) through (28) for $[0, \infty) \times \boldsymbol{D}$, where $\boldsymbol{D} = \{\boldsymbol{x} \in R^n \ | \ ||\boldsymbol{x}|| < r\}$. Thus Lemma 9.2 states that the the system response will be bounded by b, following $||\boldsymbol{x}|| \leq b$.

$$c_1||x||^2 \leq V(x) \leq c_2||x||^2, \quad (26)$$

$$\frac{\partial V}{\partial x} f(x) \leq -c_3||x||^2, \quad (27)$$

$$\left\| \frac{\partial V}{\partial x} \right\| \leq c_4||x||. \quad (28)$$

4. NUMERICAL SIMULATIONS

The simulations are carried out in the environment expressed by the process plant model derived in **Paper1** Zero perforating air leakage is assumed, i.e. all chamber walls are considered solid. The focus of the numerical simulations will be on control of roll and pitch. All the simulations below will have a fixed bias of $\boldsymbol{\beta} = 42.8$, which corresponds to the equilibrium pressure, p_0, for this vessel. The control gains will be fixed as found in section 3. All the tests will be simulated with and without the closed loop controlled system, in order to generate comparative data.

4.1 Pitch control

This section present results of numerical simulations where the system is excited with waves described in Table 1.

Table 1. Wave description

	Regular sea
Wave height, H_a	1 to 2.5 meters
Period, T_p	4 to 12 seconds
Direction, ψ	0°

Regular oncoming waves generating only pitch momentum are simulated to investigate the pitch-stabilizing properties of the closed loop controlled system. Several test are performed under the same conditions, but with varying wave periods, T_p, and wave height, H_a. The comparative results between the controlled and uncontrolled system are displayed in table 2. The detailed results for one of the simulations is displayed in Figure 3. The first plot in the Figure above displays the controlled and uncontrolled pitch angle for the simulation of $T_p = 8s$ waves. The second plot displays the valve openings of two adjacent cushions. The bottom two graphs display the pressure with and without control in one of the two aft and and one of the two rear cushions, respectively. The uncontrolled pitch has a maximum significant angle of 9.64 degrees, meaning that one third of the largest pitch angles will be 9.64 degrees
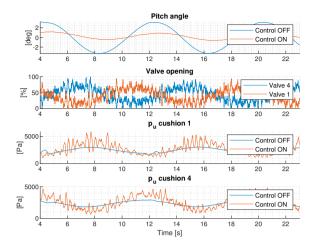
Fig. 3. Pitch angle, valve opening, cushion 1 pressure, cushion 4 pressure, for a $T_p = 8s$ wave.

peak to peak height or larger. The controlled pitch for the same case, has a significant angle of 2.11 degrees. This constitutes a 78.1% reduction of the significant peak to peak pitch angle, and a reduction of roughly 7.5 degrees from peak to peak.

Table 2. Significant angle pitch movement with control OFF/ON

T_p	H_a	H_s-OFF	H_s-ON	Damping
4s	1m	3.17	0.783	75.3 %
5s	1m	3.72	0.804	78.4 %
6s	1m	3.98	0.855	78.8 %
7s	2.5m	9.64	2.11	78.1 %
8s	2.5m	9.08	2.05	77.4 %
9s	2.5m	8.53	2.03	76.1 %
10s	2.5m	7.94	1.95	75.5 %
11s	2.5m	7.48	1.92	74.3 %
12s	2.5m	6.98	1.84	73.8 %

4.2 Roll control

This section present results of numerical simulations where the system is excited with waves described in Table 3

Table 3. Wave description

Regular sea	
Wave height, H_a	1 to 2.5 meters
Period, T_p	4 to 12 seconds
Direction, ψ	90°

The roll properties of the vessel is tested in the same way as the pitch, with a regular wave, but coming from the side. The closed loop roll movements of the vessel for one specific wave period and height can be seen in Figure 4. As with the pitch test, table 4 displays the overall results from the varying wave height and periods. The uncontrolled roll has a maximum significant angle of 15.0 degrees. The controlled pitch for the same case, has a significant angle of 2.51 degrees. This constitutes a 83.4% reduction of the significant peak to peak pitch angle, and a reduction of roughly 12.5 degrees from peak to peak.

4.3 Roll and pitch control in irregular seas

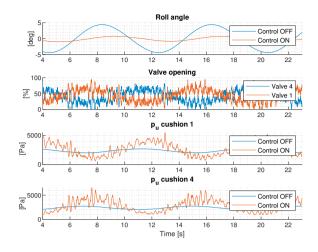The sea conditions tested in this section is given as in Table 5.

Fig. 4. Roll angle, valve opening, cushion 1 pressure, cushion 2 pressure, for a $T_p = 8s$ wave.

Table 4. Significant angle of roll movement with control OFF/ON

T_p	H_a	H_s-OFF	H_s-ON	Damping
4s	1m	9.95	1.20	88.0 %
5s	1m	9.23	1.20	87.0 %
6s	1m	7.66	1.12	85.4 %
7s	2.5m	15.0	2.51	83.4 %
8s	2.5m	12.3	2.28	81.5 %
9s	2.5m	10.2	2.10	79.5 %
10s	2.5m	8.54	1.93	77.4 %
11s	2.5m	7.29	1.78	75.5 %
12s	2.5m	6.22	1.69	72.8 %

Table 5. Wave description

JONSWAP, irregular sea	
Significant height, H_s	2.5 meters
Peak wave period, T_p	Avg. 7 seconds
Wave heading, ψ	0° to 360° at 22.5° increments
Spectral peakedness, γ	3.3

A total of 18 simulations are presented in Figure 8. Half of them are with control on, the other half with control off. Each simulation is 500 seconds long. The aim is to test simultaneous control of both pitch and roll in a realistic sea-state, and document the efficiency of the controller in various headings. The roll and pitch time series of the controlled and the uncontrolled vessel for $\psi = 135°$ can be seen in Figures 5 and 6.

The over all reduction in roll for the 360 degree wave-direction arch is 74.9%. Similarly, the error of the pitch angle is reduced by 73.1%.

The radial plot in Figure 8 shows that for angles where no roll or no pitch should occur, the control system tends to increases the roll or pitch. This is because both pitch and roll movement can be induced by the cushions via noise or small amplified excitation forces. Figure 7 displays the power spectral density (PSD) of the roll and pitch angle with and without active cushion control.

5. CONCLUSION

This paper presented active pitch and roll damping algorithm for motion regulation in a Surface Effect Ship (SES) with split cushion. The roll and pitch angles were reduced as much as 13 and 7 degrees, constituting more than a
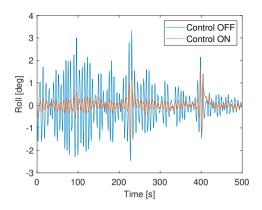
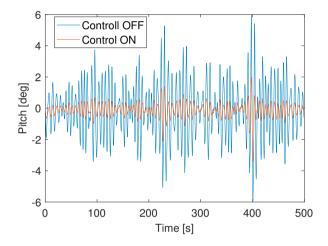Fig. 5. Roll angle with and without cushion control, $\psi = 135°$.

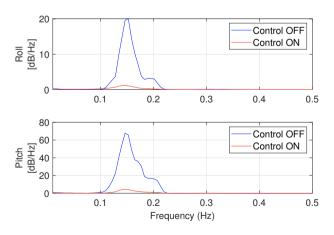Fig. 6. Pitch angle with and without cushion control, $\psi = 135°$.

Fig. 7. Roll and pitch angle power spectral density, $\psi = 135°$.

83% and 78% reduction, respectively. The roll damping is especially efficient around the roll eigenperiod of the vessel. The results are predicated on the assumption that the cushion separation walls can be seen as solid. Early experimental testing in the SINTEF Ocean's Basin with scale model of SES agrees with numerical simulations studies and shows superior performance of split cushion SES in motion regulation.
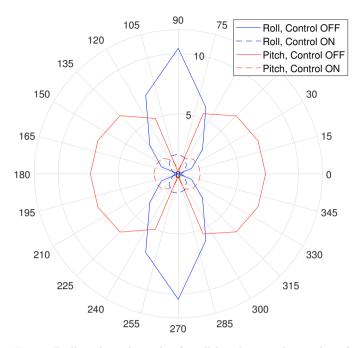

Fig. 8. Roll and pitch angles for all headings. The angles of the radial plot show $\psi[°]$. The radius shows significant roll and pitch magnitude.

REFERENCES

Kaplan, P. and S. Davis (1978). *(1978), System analysis techniques for designing ride control system for ses craft in waves.* Proceedings of the 5th Ship Contr. Syst. Symp., , Annapolis, Maryland, USA.

Sørensen, A. J. and O. Egeland (1995). "Design of Ride Control System for Surface Effect Ships using Dissipative Control". In: *Automatica* 31.2, pp. 183–199.

Khalil, Hassan K. (2014). *Nonlinear Systems, Third Edition.* Pearson Education Limited, Edinburgh Gate, Harlow, Essex CM20 2JE.

Ø. F. Auestad, Et Al. (2015). "Jan T. Gravdahl, Tristan Perez, Asgeir J. Sørensen. Boarding control system for improved accessibility to Offshore Wind Turbines: Full-scale testing". In: *Elsevier*.

Mandal, Umoe (2018). *Voyager.* URL: `URL:%20https://www.wavecraft.no/model/voyager-38x/`.

Hassani, Vahid, Snorre Fjellvang, and Ø. F. Auestad (2019). "Adaptive Boarding Control System in Surface Effect Ships". In: *Proc. of the 17th European Control Conference (ECC 2019)*. Naples, Italy.

Haukeland, Ola M., Vahid Hassani, and Ø. F. Auestad (2019). "Surface Effect Ship with Four Air Cushions, Part I: Dynamic Modeling and Simulation". In: *Proc. of the 12th IFAC Conference on Control Applications in Marine Systems, Robotics, and Vehicles (CAMS 2019)*. Daejeon, South Korea.

Haukeland, Ola Mosebø (2019). "Experimental Testing, Dynamic Modeling and Control of Roll and Pitch for a SES with a Split Cushio". MA thesis. Trondheim, Norway: Department of Marine Technology, Norwegian University of Science and Technology.